Pushing the boundaries of on-scalp magnetoencephalography towards early human life

Pierre Corvilain[1]*, Vincent Wens[1,2], Mathieu Bourguignon[3], Chiara Capparini[1,4], Lauréline Fourdin[1,4], Maxime Ferez[1], Odile Feys[1,2], Xavier De Tiège[1,2] and Julie Bertels[1,4]

[1] Laboratoire de Neuroimagerie et Neuroanatomie translationnelles (LN2T), ULB Neuroscience Institute (UNI), Université libre de Bruxelles (ULB), Brussels, Belgium

[2] CUB Hôpital Erasme, Hôpital Universitaire de Bruxelles (HUB), Université libre de Bruxelles (ULB), Brussels, Belgium

[3] Laboratory of Neurophysiology and Movement Biomechanics, ULB Neuroscience Institute (UNI), Université libre de Bruxelles (ULB), Brussels, Belgium

[4] ULBabyLab – Center for Research in Cognition and Neurosciences (CRCN), ULB Neuroscience Institute (UNI), Université libre de Bruxelles (ULB), Brussels, Belgium

*e-mail: pierre.corvilain@ulb.be

Abstract: Characterizing the early development of the human brain is critical from both fundamental and clinical perspectives. However, existing neuroimaging techniques are either not well suited to infants or have limited spatial or temporal resolution. The recent advent of optically pumped magnetometers (OPMs) has revolutionized magnetoencephalography (MEG) by enabling wearable and thus naturalistic recordings while maintaining excellent sensitivity and spatiotemporal resolution. Nevertheless, its adaptation to study brain activity in infancy poses several challenges. We present an OPM-MEG setup that successfully recorded auditory evoked responses and oddball steady-state responses reflecting auditory change detection in a group of typically developing one-month-old newborns. We thereby demonstrate the applicability of the OPM-MEG system to study early postnatal periods. These results are crucial for future OPM investigations of typical and pathological early brain development.

Keywords: magnetoencephalography, optically pumped magnetometers, newborns, auditory evoked responses, steady-states responses, frequency tagging

Introduction

During the early stages of life, the human brain undergoes major changes, with the emergence of perceptual, motor, language, and social-cognitive skills. Characterizing the neurophysiological processes underlying the development of these early abilities is crucial to understanding brain maturation and brain pathologies.

However, existing brain imaging techniques are limited in investigating early brain development. While wearable systems such as electroencephalography (EEG) and near-infrared spectroscopy (NIRS) can be adapted to small heads and enable naturalistic recordings, they have limited spatial (EEG) or temporal (NIRS) resolution. Moreover, fixed systems such as functional magnetic resonance imaging (MRI) and cryogenic magnetoencephalography (MEG) have good spatial (both) and temporal (MEG) resolution but are not adapted to—and often not well tolerated by—infants. Thus, in practice, infants are often restrained or sedated when applying these techniques.

The excellent temporal and very good spatial resolution of MEG (1) can be leveraged by having the sleeping infant rest their head on an MEG array (either using adult-size helmets in the supine position (2) or concave arrays designed to fit maternal wombs (3–6)). However, only partial head coverage can be obtained with this approach unless several recordings are performed (7). Some efforts have been made to perform whole-head MEG scans with infants. When adult-sized cryogenic MEG systems are combined with a foam halo, the infant's head can be rigidly centered in the helmet, limiting movements (8,9), but the resulting large brain-to-sensor distance is detrimental to both the signal-to-noise ratio (SNR) and spatial resolution (10). To address this issue, infant-sized cryogenic MEG systems have been developed (7); however, these systems are not usable in other age ranges and are extremely expensive, so very few systems are available worldwide (11).

Optically pumped magnetometers (OPMs) are novel magnetic field sensors that offer considerable flexibility while preserving the outstanding sensitivity of cryogenic magnetometers to the subtle magnetic fields produced by neural currents (12). In contrast to cryogenic MEG systems, in which sensors are fixed in rigid helmets, OPMs can be used to form wearable sensor arrays (OPM-MEG) that can be placed directly on the scalp, allowing for more natural and flexible scanning situations (13,14). In addition, the ensuing reduction in brain-to-sensor distance improves signal amplitude and spatial resolution (10). Crucially, a single OPM-MEG system can be adapted to all head sizes and ages, whereas several dedicated cryogenic MEG systems would be needed. OPM-MEG systems also consume less energy (direct electricity consumption; see Methods) and are more affordable than cryogenic MEG systems, which is critical for their future dissemination.

The compliance of OPM-MEG has been demonstrated over a wide range of ages, starting from two years old, for both physiological (13,15) and clinical (16,17) recordings. However, the use of OPM-MEG in younger subjects poses substantial methodological challenges. First, the surface of alkali OPMs is too warm for prolonged direct contact with the skin because the rubidium inside the sensitive cell needs to be heated to approximately 150°C (14). Therefore, due to lack of hair and skin sensitivity of newborns, efficient heat dissipation is needed to prevent discomfort and injuries. Second, multiple OPMs must be fixed on the small heads of infants to perform whole-head OPM recordings, which requires balancing ergonomics and signal quality. Recently developed triaxial OPMs increase the number of channels without impacting the ergonomics. This enables better denoising (18) and, in

infant studies where spatial sampling is limited, measurements in the direction tangential to the scalp may capture neural activity missed by measurements in the radial direction (19,20).

Here, we present a wearable OPM-MEG setup that is suitable for recordings starting from birth and demonstrate its ability to accurately characterize early brain functions in 14 one-month-old healthy neonates. We focused on auditory stimulation, as auditory evoked brain responses occur regardless of the newborn's position inside the shielded room and behavioral state (21). We established the capacity of this setup to record previously described auditory event-related responses (2). Additionally, we demonstrated its ability to record auditory steady-state potentials using a frequency tagging approach, which has never been performed in this population using MEG, and present evidence indicating oddball auditory detection. Finally, we assessed the added value of using triaxial OPMs and compared the OPM responses with those obtained from the same participants using an adult-sized cryogenic MEG. Overall, this work provides the foundation for future OPM-MEG neurodevelopmental studies in very young participants.

Results

System design. To balance the requirements of signal quality, adaptability, comfort and heat dissipation, we developed flexible EEG-like caps to which custom 3D-printed OPM holders that maintain the sensors 4 mm above the scalp were sewn (Fig. 1). The caps were equipped with ~27 small and lightweight alkali OPMs (Gen2/Gen3 QZFM, QuSpin Inc.), which almost entirely covered the scalp. As the newborns were meant to rest on their back, no sensors were placed in the occipital region. The setup was comfortable and light enough to be well tolerated by neonates during the whole experiment while resting on their parent's lap or chest. This OPM-MEG setup has previously been used by our group with a 5-month-old epileptic infant to study epileptiform discharges (22).

Fig. 1. Experimental setup. (**a**) A newborn undergoing the experiment with the OPM-MEG system. (**b**) Close-up view of the sewed-on OPM holders designed on site. The 4-mm spacing prevents direct contact between the warm OPM and the neonate scalps.

Auditory evoked responses. The aim of the first paradigm (Fig. 2a) was to demonstrate that our OPM-MEG setup can reliably detect evoked responses to pure tone stimuli. The grand-average evoked fields

in the radial direction displayed a clear response to the stimuli (Fig. 2b). The associated topographic plot exhibited the expected dipolar pattern above the bilateral temporal regions (Fig. 2c). This response was statistically significant from 179 ms to 359 ms poststimulus ($p < 10^{-4}$, maximum statistics) and its root-mean-square peaked at 261 ms. Similar analyses performed at the individual level revealed significant responses in 9 participants.

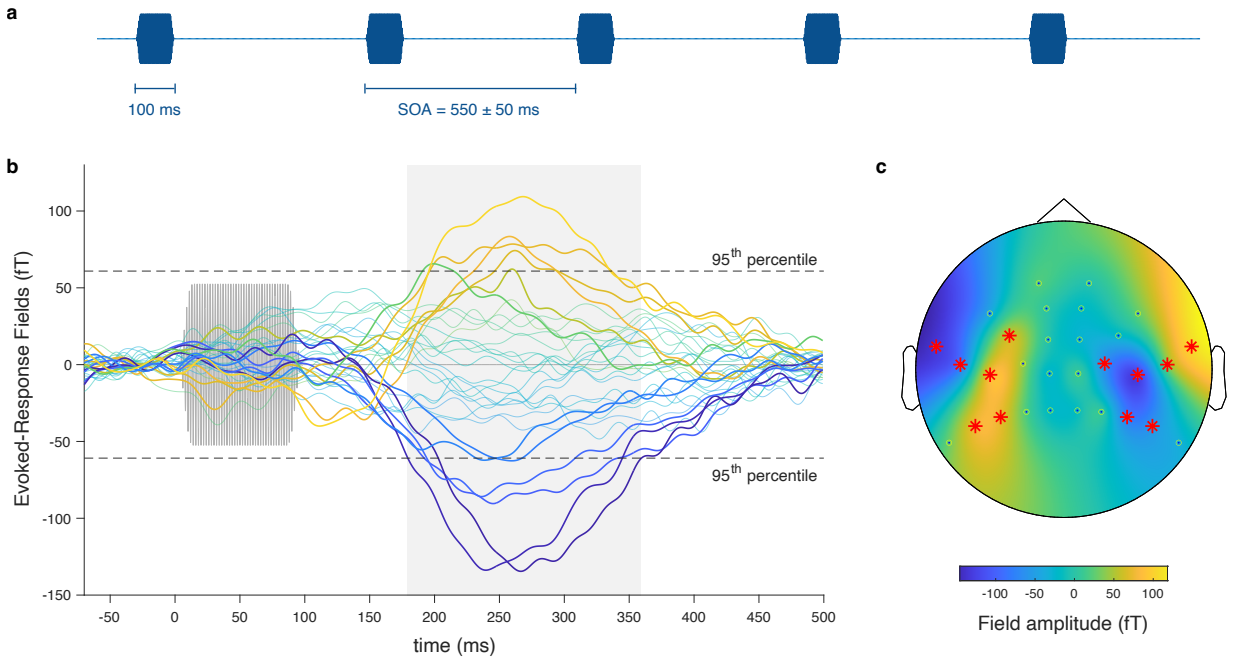

Fig. 2. Auditory evoked response paradigm. (**a**) Excerpt from the sound sequence, during which a single pure tone is presented repeatedly with a variable stimulus onset asynchrony (SOA). (**b**) Time course of the group-level evoked magnetic field measured by the OPM radial axes from -70 ms to 500 ms peristimulus. The sound stimulus is displayed in light gray (onset at 0 ms). The colors of the OPM traces match the corresponding colors on the topographic plot in panel c. Thicker traces correspond to channels showing significant responses. Periods of statistically significant responses (i.e., exceeding the 95th percentile of the surrogate distribution) are shown with a gray background. (**c**) Topographic plot of the sensors' radial axes based on their value at the moment of highest activity (determined as the maximum of the root-mean-square across all sensors, 261 ms). Sensors showing significant responses are marked with red asterisks.

Oddball responses. The aim of the second paradigm was to investigate the ability to perform a frequency tagging analysis (23,24) with newborns using the proposed OPM-MEG setup. For that purpose, a sequence of pure tones was presented at a steady 3 Hz rate in trains of 3 standard tones followed by one oddball tone (Fig. 3a). The SNR of the radial field power spectra, averaged across the participants, showed clear peaks at the base stimulation frequency (3 Hz), the oddball frequency (0.75 Hz), and its first harmonic (1.5 Hz) (Fig. 3b), suggesting the presence of steady-state responses at the base and oddball frequencies. The corresponding magnetic topographies were all compatible with cortical sources in temporal regions (Fig. 3b). Some heartbeat artifacts remained after preprocessing, leading to SNR peaks in the 2.2-2.5 Hz range, interfering with the second oddball harmonic (2.25 Hz). We performed statistical tests at 0.75 Hz, 1.5 Hz and 3 Hz and found significant SNR peaks at these frequencies ($p = 0.0016$, $p = 0.042$, and $p < 10^{-4}$, maximum statistics) for the group-averaged response and significant individual responses at those frequencies in 1, 2 and 9 participants, respectively.

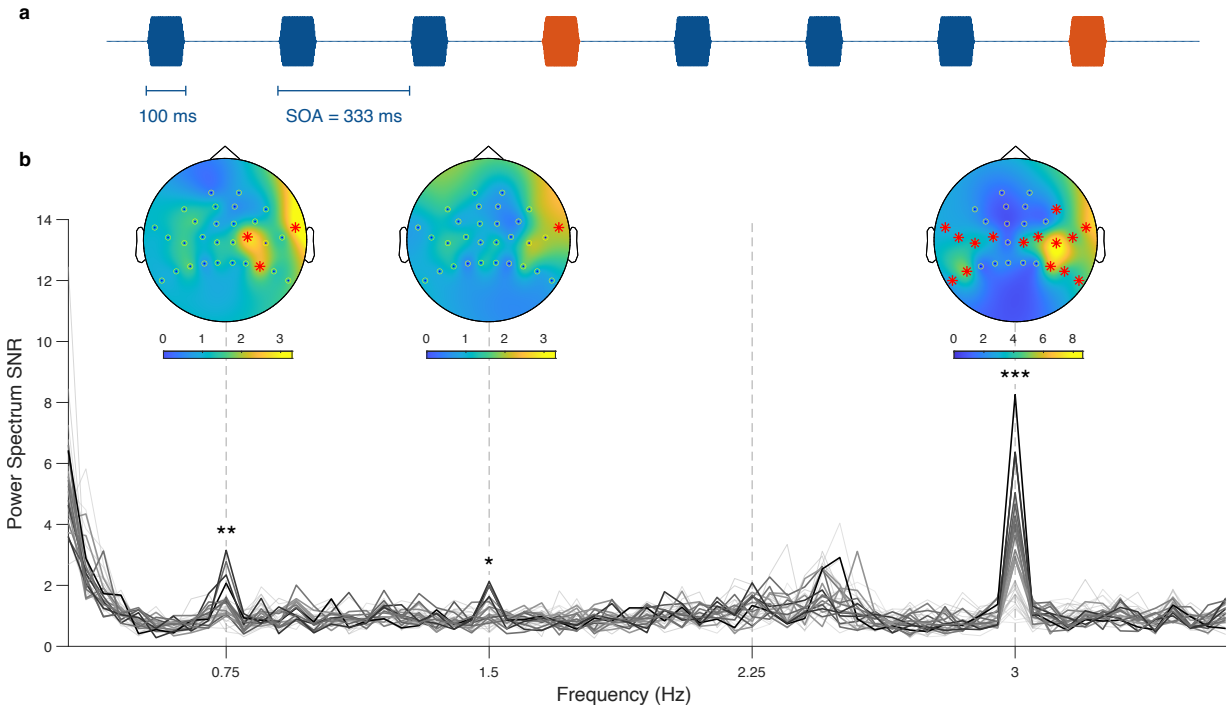

Fig. 3. Oddball paradigm. (**a**) Excerpt from the sound sequence consisting of trains of 3 base tones (blue) followed by one oddball tone (orange). The base frequency is 3 Hz, and the oddball frequency is 0.75 Hz. (**b**) Group-averaged power spectrum SNR of the OPM radial axes; the display range is 0.3-3.6 Hz. Thicker lines represent channels that were found to be significant at one of the frequencies of interest. The shade of the individual sensor curves is obtained from their SNR value at 3 Hz. Topographic plots of the SNR at the corresponding frequency are displayed above the frequencies of interest. Channels with a significant SNR are marked by red asterisks.

OPM tangential axes. For ten of the 14 participants, ~20 triaxial OPMs (Gen3 QZFM QuSpin) were available and placed over the temporal regions. In the first paradigm, the tangential component of the fields (normed and averaged across participants) displayed a clear response to the stimuli (Fig. 4a). The associated topographic plot exhibited peak activity directly above the presumed dipole source (Fig. 4b), i.e., between the two poles observed with the radial axes (Fig. 2c). This response was statistically significant from 110 ms to 364 ms poststimulus ($p < 10^{-4}$, maximum statistics) and its root-mean-square peaked at 258 ms. Individual-level analyses revealed significant responses in 7 participants. In the second paradigm, the norm of the SNR of the OPM tangential power spectra, averaged across participants, exhibited peaks at the frequencies of interest (0.75 Hz, 1.5 Hz and 3 Hz; Fig. 4c), and all peaks were significant ($p = 0.0012$, $p = 0.0007$, $p < 10^{-4}$, maximum statistics). At the individual level, the responses were significant in 3, 3 and 6 participants, respectively.

We compared the tangential and radial axes responses by evaluating the individual amplitudes and SNRs of the evoked responses and the power spectrum SNRs at the base and oddball frequencies (Fig. 5). The power spectrum SNR at 0.75 Hz was significantly higher for the tangential axes than for the radial axes ($W = 7$, $Z = -2.09$, $p = 0.037$). No other comparison was significant (all $p > 0.1$). The correlation between the amplitudes of the radial and tangential axes responses was very strong ($r = 0.9$, $p = 0.0003$).

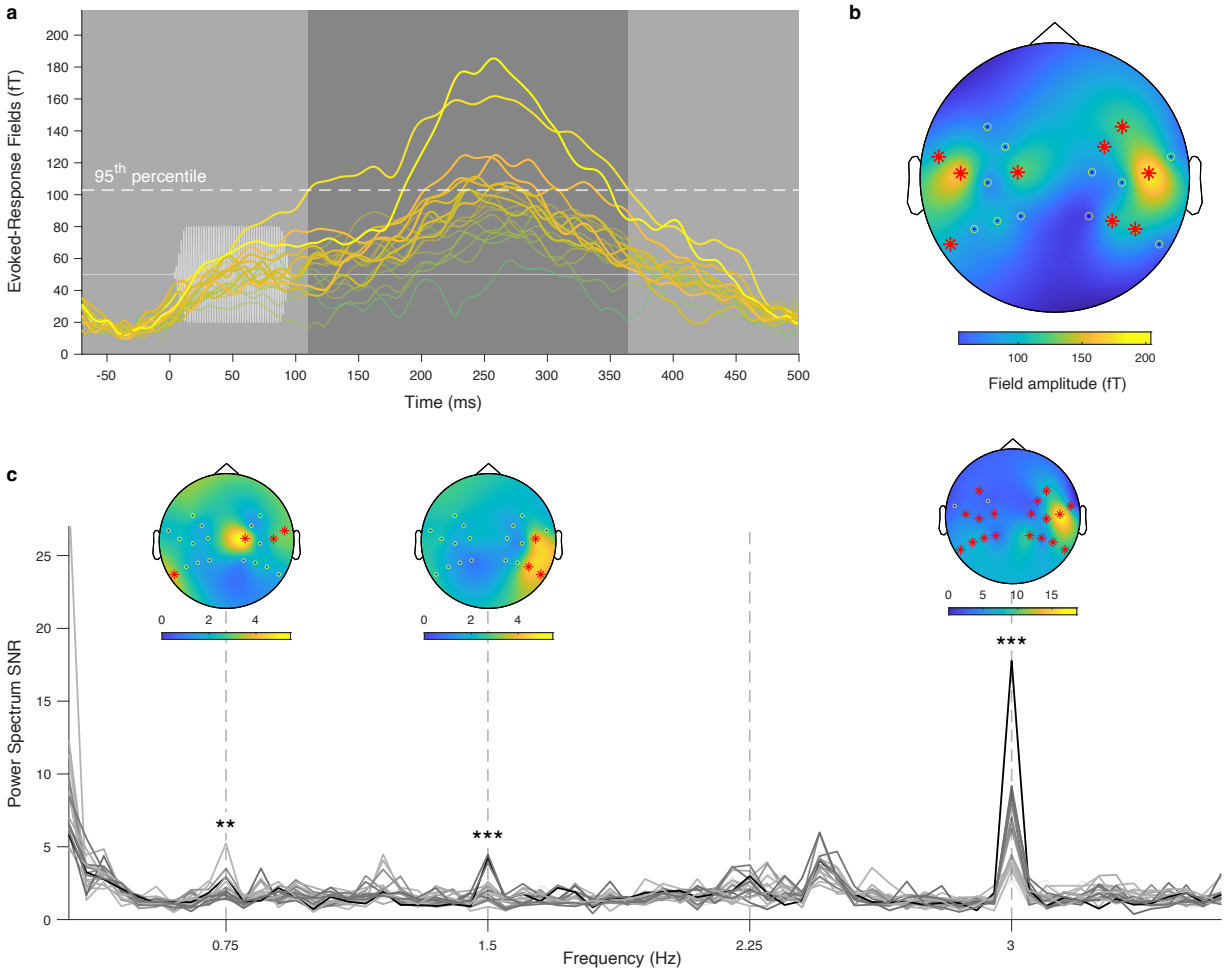

Fig. 4. **Responses in the direction tangential to the scalp** for the 10 participants that had triaxial OPMs placed over their temporal regions. (**a**) Norm of the tangential magnetic field responses to pure tones and (**b**) the associated topography at 258 ms. Note that the response amplitude peaks right above the source currents that can be inferred based on Fig. 2c. This is consistent with the fact that cortical sources yield magnetic fields that are mostly radial to the scalp in their neighborhood and tangential to the scalp right above the source. The rest of the plot is the same as in Fig. 2. (**c**) Norm of the tangential power spectrum SNRs in the oddball steady-state experiment. The rest of the plot is the same as in Fig. 3.

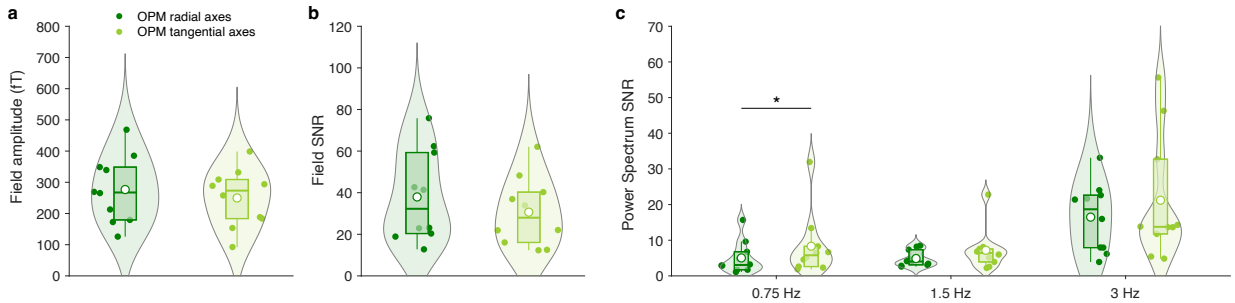

Fig. 5. Comparison of the responses recorded by the OPMs on the radial and tangential axes for the 10 participants with whom triaxial sensors were used. (**a**) Amplitude of the evoked responses, (**b**) SNR of the evoked responses and (**c**) power spectrum SNR at the frequencies of interest. The white circles represent the mean of the data. The statistical significance of the comparisons between the axial and tangential axes is indicated above the violin plots. *, $p < 0.05$.

Comparison to cryogenic MEG. A subset of 7 infants were evaluated with the same paradigms in an adult-size cryogenic MEG system (Neuromag Triux, MEGIN) in the supine position, with their head laid sideways on the posterior sensor region. Our goal was to compare the recordings obtained using both modalities. The root-mean-square of the averaged auditory evoked responses peaked at 264 ms poststimulus with the OPM-MEG and at 282 ms with the cryogenic MEG. We compared the amplitudes and SNRs of the evoked responses and the power spectrum SNRs at the base and oddball frequencies (Fig. 6). The amplitude of the evoked responses was significantly higher (on average ~4 times higher) with OPM-MEG than with cryogenic MEG ($t(6) = 8.05$, $p = 0.0002$), as expected due to the reduced brain-to-sensor distance. The SNRs of both the evoked responses and the power spectrum were not significantly different (all $p > 0.26$).

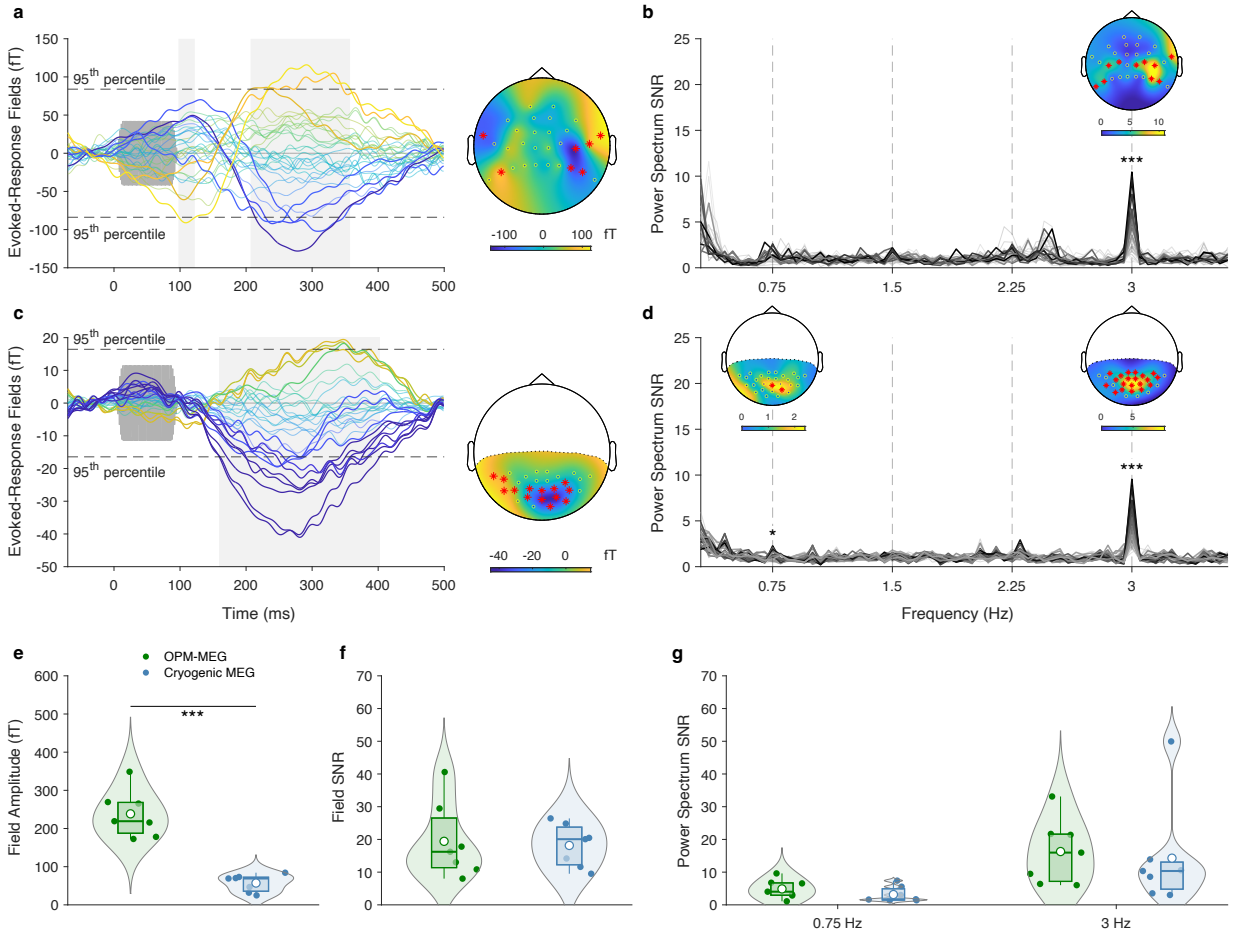

Fig. 6. Comparison of the OPM-MEG and cryogenic MEG systems for the 7 participants who underwent the experiments with both modalities. (**Left**) Radial magnetic fields evoked in response to single tones measured with (**a**) OPM-MEG and (**c**) cryogenic MEG. The plots are the same as in Fig. 2. Unsurprisingly, given that the infants were lying on their sides in the cryogenic MEG setup, we observed a single dipole in the posterior cryogenic sensors. We also show a comparison of (**e**) the amplitude of the evoked response and (**f**) their SNR. (**Right**) Radial magnetic field spectrum SNR for the steady-state response obtained with (**b**) OPM-MEG and (**d**) cryogenic MEG. All is the same as in Fig. 3. (**g**) The power spectrum SNRs are compared at 0.75 Hz and 3 Hz. The white circles represent the mean of the data. The statistical significance of the comparisons between OPM and cryogenic MEG is indicated above the violin plots. ***, $p < 0.001$.

Discussion

In this work, we developed a wearable whole-head OPM-MEG setup that fits and is well tolerated by newborns. Our design, which used flexible EEG-like caps and slightly elevated OPM holders, prevented heat-related discomfort to the neonates' skin. Compared to cryogenic MEG, the sensors are closer to the scalp in our setup, resulting in signals with higher amplitudes. Importantly, data can be acquired in a setting that is more naturalistic and appropriate for newborns, with the baby resting comfortably on their parent's lap. These advantages are likely unachievable with one-size-fits-most rigid helmets, as used in previous OPM studies (15). Thus, our OPM-MEG setup has the advantages of both approaches: the flexibility and applicability to newborns of wearable systems such as EEG and the high spatial precision of MEG. OPM-MEG systems are also more affordable and less energy intensive than cryogenic MEG systems (46-48). In addition, our setup can be easily adapted to older participants (see (16,17) for studies in school-aged children), making it an MEG system that is applicable across all ages.

We demonstrated that OPM-MEG can acquire high-quality data by performing two auditory paradigms with a group of one-month-old healthy newborns. The system successfully and accurately recorded the 250-ms response to pure tones, as previously reported in the cryogenic MEG (2–5) and EEG (25–27) literature; in the latter, it is known as the P2 component (27). The associated magnetic topography was compatible with sources in the auditory cortex. The OPM-MEG system also demonstrated the possibility of applying frequency tagging paradigms with newborns, which have been shown to be very fruitful with young participants (24,28). Frequency tagging paradigms similar to the one applied in this study were carried out with EEG in adults (29) and infants (30–32), but to our knowledge, infant steady-state responses have not yet been studied with MEG or in response to tone frequency changes. The existence of significant peaks in the power spectrum SNR at the oddball frequency and its first harmonic is a frequency tagging analog of the auditory mismatch negativity (MMN), which reflects automatic change detection (33). In the frequency tagging approach, these peaks can also reveal rhythm perception and, more generally extraction of structural patterns (30–32), as the trains of stimuli are presented periodically. Interestingly, the magnetic topographies suggest right-lateralized cortical sources for these oddball responses, echoing previous observations in 2-month-olds (34). Notably, observing the SNR peak in the spectrum at 0.75 Hz is a nontrivial feat of our system, as the OPM signal is known to be very noisy at such low frequencies due to movement and ambient field drifts (13), and dealing with this low-frequency noise has rarely been performed (35). Finally, we showed that neural activity can be accurately recorded in the direction tangential to the scalp in this population and that, in some instances, these axes are better suited to uncover significant responses. In our setup, similar activity was captured in the radial and tangential directions, as seen from the high correlation between the response amplitudes; however, this might not be the case for setups designed for smaller heads, such as those for preterm neonates.

There are some limitations to our study. First, we did not measure the exact positions and orientations of the sensors on the newborns' heads, for none of the available methods were suitable. When using a 3D scanner (17) or an electromagnetic tracker (16,22), the neonates must be placed in constraining positions with all sensors clearly accessible, where the orientations of the OPMs might differ substantially from the recording position. The prime solution would be magnetic localization using additional coils (36–38). This approach would allow source reconstruction with the OPM-MEG system, thereby taking full advantage of its better spatial resolution and lower signal distortion due to sutures

and fontanels compared to EEG (39). Second, a disadvantage of on-scalp OPM-MEG is that movements lead to high-amplitude artifacts due to the OPMs moving in a nonzero magnetic field. This can be addressed by keeping the ambient field as low as possible, which requires magnetic shielding and the use of field-nulling coils, as applied in our study; however, a small magnetic field always remains. Further improvements in interference suppression techniques (40,41) will likely increase the SNR of OPM data which may exceed that of cryogenic MEG data. Indeed, in our comparison between OPM-MEG and cryogenic MEG, we found similar SNRs despite the significantly higher signal amplitude with OPM-MEG.

Based on our data, we suggest that additional OPM-MEG studies on very early brain development would be useful, as these studies would especially benefit from the naturalness of the proposed wearable system and the increased signal amplitude with the on-scalp sensors. An interesting prospect would be to use the OPM-MEG system to record activity in premature newborns, thereby assessing human brain development before term (32). Another compelling perspective would be to adapt the proposed OPM-MEG setup to the wombs of pregnant women for fetal MEG. Successful recordings of fetal evoked responses have been achieved using expensive dedicated cryogenic MEG systems (42). While OPMs are capable of fetal magnetocardiography (43), their use for fetal MEG could be far-reaching for studying prenatal brain development. The present study is a called-for first step in this research direction.

In conclusion, the present study reports an innovative wearable MEG system that allows for naturalistic recordings in neonates. This research paves the way for further early neurodevelopmental investigations in natural situations using OPM-MEG, which may ultimately provide a wealth of unprecedented information on brain functional maturation starting from birth. Arguably, this is also a step toward OPM-MEG becoming a fundamental clinical tool for evaluating newborns and infants.

Materials and Methods

Participants. Fourteen neonates (7 females) participated in this study; their ages ranged between 29 and 36 days (mean: 32.6 days)**.** The inclusion criteria were as follows: gestational age >36 weeks, APGAR scores >7 at 5 and 10 minutes after birth, uncomplicated pregnancy, no known developmental delay, and normal hearing at birth (cf. otoacoustic emissions). For each paradigm, we had to reject the data of one participant (a different participant in each dataset) due to technical issues. The parents gave informed consent prior to testing and received monetary compensation for their participation. The CUB Hôpital Erasme Ethics Committee approved the experimental protocol (P2021/141/B406202100081). The methods were carried out in accordance with the approved guidelines and regulations.

System design and data acquisition. To build a wearable OPM-MEG system that was suitable for newborns, we used flexible and slightly stretchy caps (EasyCap, sizes: 36, 38 and 40 cm of head circumference), onto which we sewed OPM holders that we designed and 3D-printed with acrylonitrile butadiene styrene (ABS) on site. As a result, the interior of the cap was fabric, and the cap was comfortable to wear. The holders were set so that a gap of 4 mm was left between the scalp and the OPM (Fig. 1b), which is crucial to dissipate the heat generated by the rubidium-based OPMs and prevent hurting the sensitive skin of newborns. Indeed, the rubidium inside the sensitive cell needs to be heated to approximately 150°C to work in the spin exchange relaxation-free regime (44), making the OPM surface relatively hot. Notably, helium-based OPMs do not heat (45); however, to date, He-

OPMs are too heavy and bulky (20) to be placed on a newborn scalp, as opposed to the OPMs used in this study (size: 1.2 x 1.7 x 2.6 cm^3, weight: 4.5–4.7 g). In addition, we attached aerogel foam to the bottom of the OPMs to further isolate the scalp. The caps were equipped with 19 to 30 (mean: 27) biaxial or triaxial OPMs (Gen2/Gen3 QZFM, QuSpin Inc.), depending on the cap size and OPM availability. The 15 to 24 triaxial sensors (mean: 20, available for 10 participants) were placed in priority over the temporal areas to increase sensitivity to auditory responses (10,18). When wearing the cap, the newborns could rest on the laps of one of their parents, seated inside a magnetically shielded room (Compact MuRoom, MSL Ltd). The room was degaussed and wall coils (MuCoils, Cerca Magnetics) were used—available for 10 participants—in order to further reduce the remanent magnetic fields below 1 nT within a 40-cm wide cubic region of interest containing the newborn's head. This was achieved by mapping, before the acquisition, the remanent static magnetic field in that cube using the offset-corrected field-zero values of ~20 triaxial OPMs positioned in that region using a custom-made all-wood structure. The magnetic profiles of the coils were determined at those positions by sending voltages in step pulses and measuring the magnetic responses with the OPMs. The latter were then inverted to null the magnetic field measured in the previous step. The sound sequences were presented using an MEG-compatible flat wall speaker (Panphonics). Data were recorded at a sampling frequency of 1200 Hz using a 16-bit digital acquisition (DAQ) system (National Instruments) controlled by a custom-made Python program. Audio stimuli were recorded simultaneously with the DAQ. If needed, the infants used a nonmagnetic pacifier. Live video was available during the whole experiment to monitor and address any problems that may have occurred. ***Direct energy consumption***. The OPMs (QuSpin Inc.) have a total direct power consumption of 5 W per sensor (46) and can be switched off when not in use. A high-density array of 128 OPMs (384 channels) used for 7 hours in one day would thus consume 4.4 kWh of electricity. For comparison, the 306-channel cryogenic MEG TRIUX neo (MEGIN) system has a minimum power consumption of 4.2 kW (47) and cannot be switched off. It therefore consumes a minimum of 100.8 kWh of electricity in one day. Taking the helium recycler (48) and the type of current used into account, the daily consumption ranges between 110 and 190 kWh. We report here only the direct energy consumption, as no life cycle analysis of both MEG types has been performed.

Auditory stimuli. Both auditory paradigms consisted of 5-minute sequences of 100 ms pure tones at 65 dB with 15 ms of fade-in and fade-out. We presented each type of sequence more than once—when possible—to increase the amount of data (total number of sequences presented: 2-5, mean: 3) in a randomized order. ***Evoked response paradigm.*** In each sequence, a single pure tone with a frequency of either 500 or 750 Hz (depending on the sequence) was presented with a stimulus onset asynchrony (SOA) randomly varying between 500 and 600 ms (Fig. 2a). ***Oddball paradigm.*** Pure tones were presented at a steady 3 Hz rate in trains of 3 base tones followed by one oddball tone, leading to an oddball frequency of 0.75 Hz (Fig. 3a); this paradigm was inspired by (29). The base (oddball) tone frequency was either 500 or 750 Hz (750 or 500 Hz), depending on the sequence. For both paradigms, the different sequence types were treated identically for the analysis.

Data analysis. *Preprocessing*. Recording periods containing large movement artifacts were first identified by visual inspection and marked as artifact time windows. Heartbeat artifacts from the newborn and the parent were then removed with an independent component analysis (ICA) (49) using the FastICA algorithm (50), which was applied to the non-artifacted part of the recordings, which were bandpass filtered between 1-40 Hz. Time windows affected by remaining artifacts were identified by visual examination of the other independent components by sliding through 5-second windows.

Evoked response paradigm. Data in the artifact periods were replaced by linear interpolation, then bandpass filtered between 1-40 Hz, and notch filtered at the frequencies at which the power spectrum displayed noise peaks, within the 13-40 Hz range. Artifact periods were then extended by 1.5 s in both directions. A robust z-score rejection (channel per channel, threshold value of 5, data amplitude smoothed with a 1 s square window beforehand) was then performed to identify time stamps affected by remaining artifacts. The first three principal components of the artifact-free data were then projected out (16). The resulting data were decomposed into epochs from -70 to 500 ms around the start of each sound presentation, and epochs that intersected artifact periods were rejected. The remaining epochs were baseline corrected with a baseline spanning the 70 ms prestimulus period. The epochs were averaged for each participant (individual-level evoked response). The norm of the response along the tangential direction was taken. Finally, the evoked responses were averaged across all participants (group-level). ***Oddball paradigm*.** The data were bandpass filtered between 0.2-40 Hz (to maintain access to the oddball frequency), and notch filtered at the frequencies at which the power spectrum displayed noise peaks, within the 13-40 Hz range. The first three principal components estimated from the artifact-free data were then projected out. The ranges of the newborn's and parent's heart rates were computed based on the components identified in the ICA preprocessing, and further components containing heartbeat artifacts were removed if, in those heart frequency ranges, their power spectrum SNR (computed as explained below) exceeded 7.5. The resulting data were decomposed into artifact-free, 20-s epochs, starting when an oddball sound was presented to preserve the stimulus-related temporal structure across epochs. The complex-valued Fourier coefficients of the data in each epoch were computed using the fast Fourier transform algorithm and averaged across epochs. The power spectrum was obtained as the squared magnitude of the resulting Fourier coefficients. Then, the SNR was computed for each frequency bin as the ratio of the power at that frequency to the mean power across the two 0.1-0.4 Hz frequency intervals around the considered frequency. The tangential SNR was computed as the norm of the SNRs in the 2 tangential directions. Group-level SNRs were obtained by averaging across participants. ***Cryogenic MEG***. Data were first denoised using signal space separation (MaxFilter, MEGIN) without movement compensation, as the head position was not tracked. Only the magnetometer data were retained, and all the other steps were the same as those for processing the OPM-MEG data, except that the three first principal components were not removed. ***Topographies*.** Topographic plots were generated using Fieldtrip (51) and group averages were performed on the basis of a 2D layout that most closely matched the sensor positions for all the different cap sizes used.

Statistics. Maximum statistics tests were performed on the evoked and steady-state responses at both the individual and group levels, hence providing full control of the familywise error rate. The iterative *step-down method* (52) was used, i.e., data that were found to be significant in one iteration were masked off the maximum statistics test in the next iteration until no more significant data were found. The statistical significance level was set to $p < 0.05$. Null distributions were constructed from 10,000 samples of surrogate data built according to the null hypothesis that they contain no response to the stimuli. For the evoked responses in the time domain, the sign of each epoch was randomly flipped (permutation test), and for the frequency tagging analysis, the phases of Fourier coefficients were randomly changed. In both cases, the same changes were applied to all OPM channels to preserve their spatial distribution. To compare the different modalities (radial versus tangential axes, n = 10, and OPM versus cryogenic MEG, n = 7), we performed two-tailed paired sample *t*-tests, unless Shapiro–Wilk tests indicated that the distributions deviated from normality, in which case two-tailed

Wilcoxon signed-rank tests were performed. For these tests, the amplitude of the evoked responses was computed as the highest value across the channels at the point where the root-mean-square of all channels peaked. The SNR for these evoked responses was computed as the ratio between the amplitude and the standard deviation of this channel time-series during the baseline (70 ms prestimulus period). Finally, the individual power spectrum SNR for the steady-state responses was taken as the highest power spectrum SNR value at each of the frequencies of interest.

References

1. Baillet S. Magnetoencephalography for brain electrophysiology and imaging. Nat Neurosci. 2017;20: 327–339.
2. Huotilainen M, Kujala A, Hotakainen M, Shestakova A, Kushnerenko E, Parkkonen L, et al. Auditory magnetic responses of healthy newborns. Neuroreport. 2003;14: 1871–1875.
3. Lengle JM, Chen M, Wakai RT. Improved neuromagnetic detection of fetal and neonatal auditory evoked responses. Clin Neurophysiol. 2001;112: 785–792.
4. Holst M, Eswaran H, Lowery C, Murphy P, Norton J, Preissl H. Development of auditory evoked fields in human fetuses and newborns: a longitudinal MEG study. Clin Neurophysiol. 2005;116: 1949–1955.
5. Draganova R, Eswaran H, Murphy P, Lowery C, Preissl H. Serial magnetoencephalographic study of fetal and newborn auditory discriminative evoked responses. Early Hum Dev. 2007;83: 199–207.
6. Muenssinger J, Matuz T, Schleger F, Kiefer-Schmidt I, Goelz R, Wacker-Gussmann A, et al. Auditory habituation in the fetus and neonate: an fMEG study. Dev Sci. 2013;16: 287–295.
7. Chen Y-H, Saby J, Kuschner E, Gaetz W, Edgar JC, Roberts TPL. Magnetoencephalography and the infant brain. Neuroimage. 2019;189: 445–458.
8. Clarke MD, Larson E, Peterson ER, McCloy DR, Bosseler AN, Taulu S. Improving Localization Accuracy of Neural Sources by Pre-processing: Demonstration With Infant MEG Data. Front Neurol. 2022;13: 827529.
9. Clarke MD, Bosseler AN, Mizrahi JC, Peterson ER, Larson E, Meltzoff AN, et al. Infant brain imaging using magnetoencephalography: Challenges, solutions, and best practices. Hum Brain Mapp. 2022;43: 3609–3619.
10. Wens V. Exploring the limits of MEG spatial resolution with multipolar expansions. Neuroimage. 2023;270: 119953.
11. Feys O, De Tiège X. From cryogenic to on-scalp magnetoencephalography for the evaluation of paediatric epilepsy. Dev Med Child Neurol. 2023. doi:10.1111/dmcn.15689
12. Boto E, Meyer SS, Shah V, Alem O, Knappe S, Kruger P, et al. A new generation of magnetoencephalography: Room temperature measurements using optically-pumped magnetometers. Neuroimage. 2017;149: 404–414.
13. Boto E, Holmes N, Leggett J, Roberts G, Shah V, Meyer SS, et al. Moving magnetoencephalography towards real-world applications with a wearable system. Nature. 2018;555: 657–661.

14. Brookes MJ, Leggett J, Rea M, Hill RM, Holmes N, Boto E, et al. Magnetoencephalography with optically pumped magnetometers (OPM-MEG): the next generation of functional neuroimaging. Trends Neurosci. 2022;45: 621–634.

15. Hill RM, Boto E, Holmes N, Hartley C, Seedat ZA, Leggett J, et al. A tool for functional brain imaging with lifespan compliance. Nat Commun. 2019;10: 4785.

16. Feys O, Corvilain P, Aeby A, Sculier C, Holmes N, Brookes M, et al. On-Scalp Optically Pumped Magnetometers versus Cryogenic Magnetoencephalography for Diagnostic Evaluation of Epilepsy in School-aged Children. Radiology. 2022;304: 429–434.

17. Feys O, Corvilain P, Van Hecke A, Sculier C, Rikir E, Legros B, et al. Recording of Ictal Epileptic Activity Using on-Scalp Magnetoencephalography. Ann Neurol. 2023;93: 419–421.

18. Brookes MJ, Boto E, Rea M, Shah V, Osborne J, Holmes N, et al. Theoretical advantages of a triaxial optically pumped magnetometer magnetoencephalography system. Neuroimage. 2021;236: 118025.

19. Boto E, Shah V, Hill RM, Rhodes N, Osborne J, Doyle C, et al. Triaxial detection of the neuromagnetic field using optically-pumped magnetometry: feasibility and application in children. Neuroimage. 2022;252: 119027.

20. Feys O, Corvilain P, Labyt E, Mahmoudzadeh M, Routier L, Sculier C, et al. Tri-axial rubidium and helium optically pumped magnetometers for on-scalp magnetoencephalography recording of interictal epileptiform discharges: A case study. Front. Neurosci. 2023; 17

21. Martynova O, Kirjavainen J, Cheour M. Mismatch negativity and late discriminative negativity in sleeping human newborns. Neurosci Lett. 2003;340: 75–78.

22. Feys O, Corvilain P, Bertels J, Sculier C, Holmes N, Brookes M, et al. On-scalp magnetoencephalography for the diagnostic evaluation of epilepsy during infancy. Clin Neurophysiol. 2023;155: 29–31.

23. Regan D. COMPARISON OF TRANSIENT AND STEADY-STATE METHODS*. Ann N Y Acad Sci. 1982;388: 45–71.

24. Kabdebon C, Fló A, de Heering A, Aslin R. The power of rhythms: how steady-state evoked responses reveal early neurocognitive development. Neuroimage. 2022;254: 119150.

25. Shibasaki H, Miyazaki M. Event-related potential studies in infants and children. J Clin Neurophysiol. 1992;9: 408–418.

26. Wunderlich JL, Cone-Wesson BK, Shepherd R. Maturation of the cortical auditory evoked potential in infants and young children. Hear Res. 2006;212: 185–202.

27. Fellman V, Huotilainen M. Cortical auditory event-related potentials in newborn infants. Semin Fetal Neonatal Med. 2006;11: 452–458.

28. Bertels J, Bourguignon M, de Heering A, Chetail F, De Tiège X, Cleeremans A, et al. Snakes elicit specific neural responses in the human infant brain. Sci Rep. 2020;10: 7443.

29. Nozaradan S, Mouraux A, Cousineau M. Frequency tagging to track the neural processing of contrast in fast, continuous sound sequences. J Neurophysiol. 2017;118: 243–253.

30. Cirelli LK, Spinelli C, Nozaradan S, Trainor LJ. Measuring Neural Entrainment to Beat and Meter in Infants: Effects of Music Background. Front Neurosci. 2016;10: 229.

31. Lenc T, Peter V, Hooper C, Keller PE, Burnham D, Nozaradan S. Infants show enhanced neural responses to musical meter frequencies beyond low-level features. Dev Sci. 2023;26: e13353.

32. Edalati M, Wallois F, Safaie J, Ghostine G, Kongolo G, Trainor LJ, et al. Rhythm in the Premature Neonate Brain: Very Early Processing of Auditory Beat and Meter. J Neurosci. 2023;43: 2794–2802.

33. Näätänen R, Paavilainen P, Rinne T, Alho K. The mismatch negativity (MMN) in basic research of central auditory processing: a review. Clin Neurophysiol. 2007;118: 2544–2590.

34. He C, Hotson L, Trainor LJ. Mismatch responses to pitch changes in early infancy. J Cogn Neurosci. 2007;19: 878–892.

35. de Lange P, Boto E, Holmes N, Hill RM, Bowtell R, Wens V, et al. Measuring the cortical tracking of speech with optically-pumped magnetometers. Neuroimage. 2021;233: 117969.

36. Pfeiffer C, Andersen LM, Lundqvist D, Hämäläinen M, Schneiderman JF, Oostenveld R. Localizing on-scalp MEG sensors using an array of magnetic dipole coils. PLoS One. 2018;13: e0191111.

37. Pfeiffer C, Ruffieux S, Andersen LM, Kalabukhov A, Winkler D, Oostenveld R, et al. On-scalp MEG sensor localization using magnetic dipole-like coils: A method for highly accurate co-registration. Neuroimage. 2020;212: 116686.

38. Iivanainen J, Borna A, Zetter R, Carter TR, Stephen JM, McKay J, et al. Calibration and Localization of Optically Pumped Magnetometers Using Electromagnetic Coils. Sensors . 2022;22. doi:10.3390/s22083059

39. Lew S, Sliva DD, Choe M-S, Grant PE, Okada Y, Wolters CH, et al. Effects of sutures and fontanels on MEG and EEG source analysis in a realistic infant head model. Neuroimage. 2013;76: 282–293.

40. Seymour RA, Alexander N, Mellor S, O'Neill GC, Tierney TM, Barnes GR, et al. Interference suppression techniques for OPM-based MEG: Opportunities and challenges. Neuroimage. 2022;247: 118834.

41. Holmes N, Bowtell R, Brookes MJ, Taulu S. An Iterative Implementation of the Signal Space Separation Method for Magnetoencephalography Systems with Low Channel Counts. Sensors . 2023;23. doi:10.3390/s23146537

42. Keune J, Eswaran H, Preissl H. Fetal Magnetoencephalography (fMEG). Magnetoencephalography. 2019; 661–676.

43. Wakai R. Fetal Magnetocardiography with OPMs. In: Labyt E, Sander T, Wakai R, editors. Flexible High Performance Magnetic Field Sensors: On-Scalp Magnetoencephalography and Other Applications. Cham: Springer International Publishing; 2022. pp. 283–297.

44. Tierney TM, Holmes N, Mellor S, López JD, Roberts G, Hill RM, et al. Optically pumped magnetometers: From quantum origins to multi-channel magnetoencephalography. Neuroimage. 2019;199: 598–608.

45. Gutteling TP, Bonnefond M, Clausner T, Daligault S, Romain R, Mitryukovskiy S, et al. A New Generation of OPM for High Dynamic and Large Bandwidth MEG: The He OPMs-First Applications in Healthy Volunteers. Sensors . 2023;23. doi:10.3390/s23052801

46. http://quspin.com/products-qzfm/

47. https://megin.com/wp-content/uploads/2022/01/MEGIN-TRIUX-neo-Product-Data-2021.pdf

48. https://megin.com/wp-content/uploads/2022/01/MEGIN-Internal-Helium-Recycler-2021.pdf

49. Vigário R, Särelä J, Jousmäki V, Hämäläinen M, Oja E. Independent component approach to the analysis of EEG and MEG recordings. IEEE Trans Biomed Eng. 2000;47: 589–593.

50. A. Hyvarinen. Fast ICA for noisy data using Gaussian moments. 1999.

51. Oostenveld R, Fries P, Maris E, Schoffelen J-M. FieldTrip: Open source software for advanced analysis of MEG, EEG, and invasive electrophysiological data. Comput Intell Neurosci. 2011;2011: 156869.

52. Nichols TE, Holmes AP. Nonparametric permutation tests for functional neuroimaging: a primer with examples. Hum Brain Mapp. 2002;15: 1–25.

Acknowledgments

Funding: Fonds Erasme, Convention « Alzheimer » (PC, MF)
Fondation Jaumotte-Demoulin grant (JB)
FRS-FNRS Incentive grant for scientific research F.4503.22 (JB, CC, LF)
FRS-FNRS FRIA grant (OF)
Engineering and Physical Sciences Research Council grant (MB)
Fonds Erasme, Projet de Recherche Clinique
Fonds Erasme, Convention « Les Voies du Savoir 1 & 2 »
FRS-FNRS Research grant J.0043.20F
FRS-FNRS Equipment grant U.N013.21F

Author contributions: Conceptualization: PC, JB
Methodology: PC
Software: PC
Formal analysis: PC, VW, MB
Investigation: PC, JB, CC, LF, MF
Resources: XDT, OF
Data Curation: PC
Writing—original draft: PC
Writing—review & editing: PC, JB, VW, MB, XDT, CC, MF, LF
Visualization: PC
Supervision: JB, XDT

Competing interests: All the authors declare that they have no competing interests.

Data and materials availability: All data, code and materials used in the analyses are available upon reasonable request from the corresponding author.